Electronic Supplementary Material (ESI) for Dalton Transactions.

Supporting Information

Investigation on in situ sulfide/nitride/phosphide treatments of hematite photoanodes for improved solar water oxidation

Xiu-Shuang Xing,[a] Zhongyuan Zhou,*[b] Peilin Song,[a] Xin Song,[b] Xiaofei Ren,[a,c] Daojun Zhang,[a] Xuyang Zeng,[a,c] Yao Guo,[b] and Jimin Du*[a,c]

[a]International Joint Laboratory of Henan Photoelectric Functional Materials, College of Chemistry and Chemical Engineering, Anyang Normal University, Anyang 455000, P. R. China. E-mail: djm@iccas.ac.cn

[b]Henan International Joint Research Laboratory of Nanocomposite Sensing Materials, Anyang Institute of Technology, Anyang 455000, China. Email: 20200038@ayit.edu.cn

[c]College of Chemistry, Zhengzhou University, Zhengzhou 450000, P. R. China.

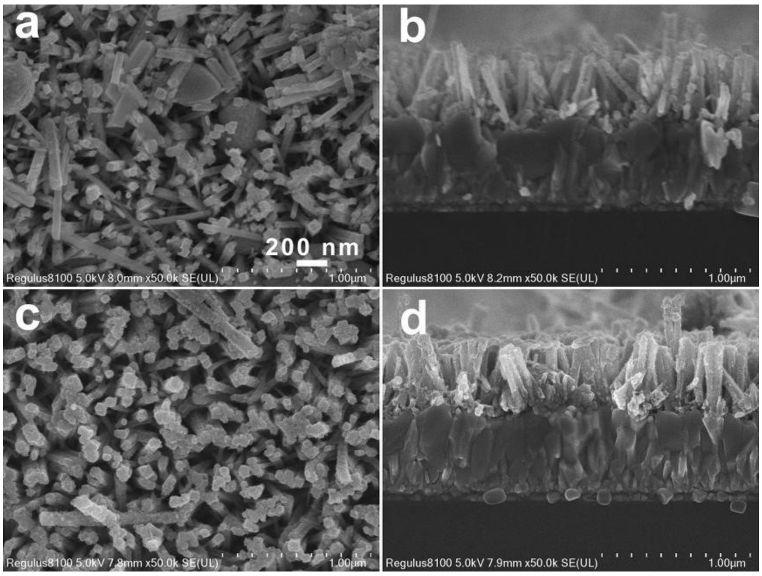

Fig. S1 The top-views and cross-section SEM images of FTO/Sn@α-Fe_2O_3 (**a** and **b**) and FTO/Sn@α-Fe_2O_3/FeOOH (**c** and **d**) photoanodes.

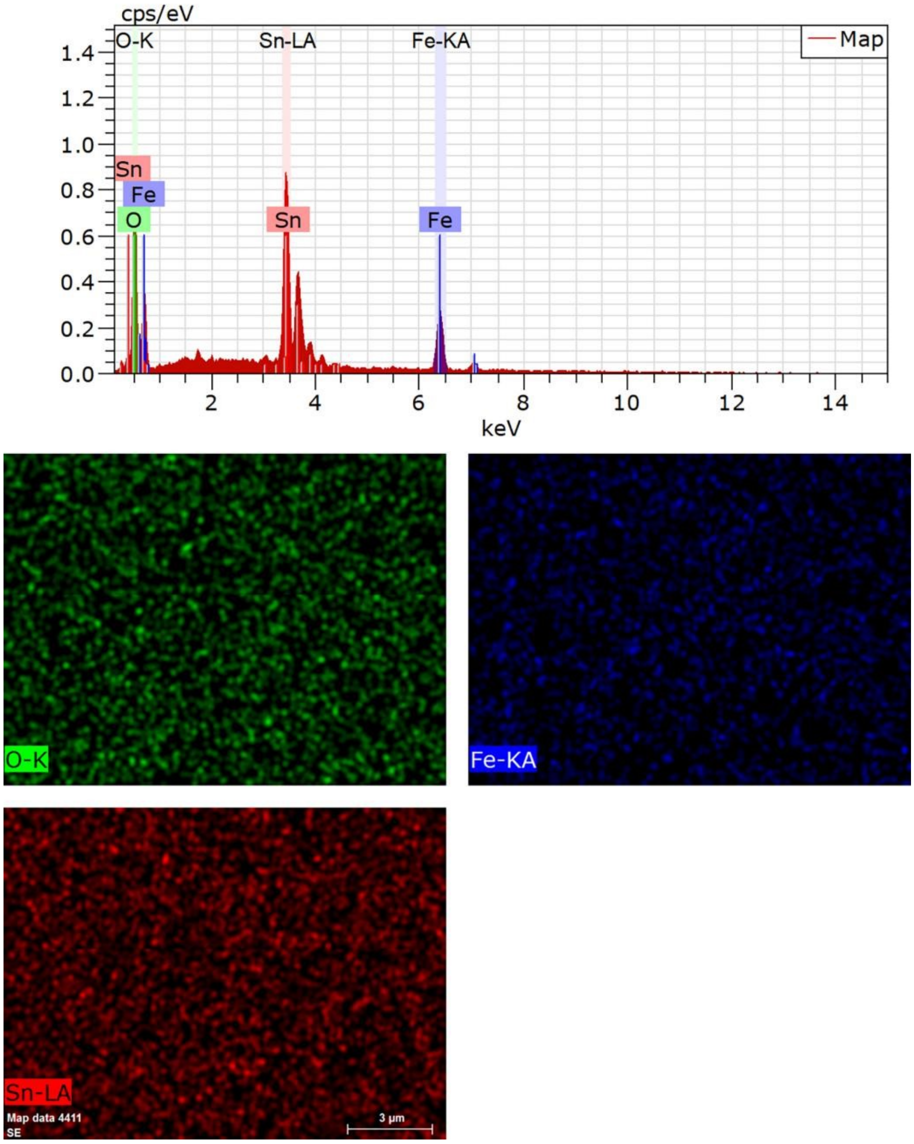

Fig. S2 The EDS composition of FTO/Sn@α-Fe_2O_3 photoanode.

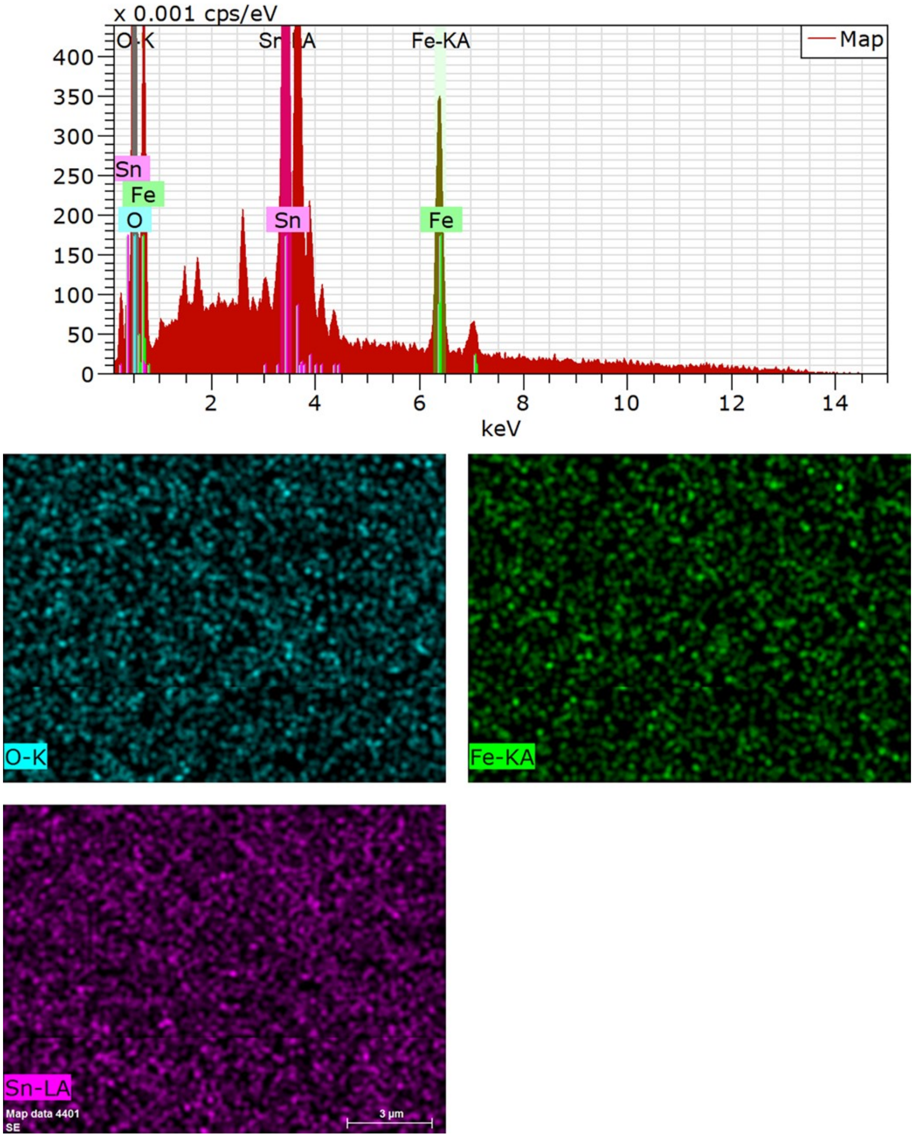

Fig. S3 The EDS composition of FTO/Sn@α-Fe_2O_3/FeOOH photoanode.

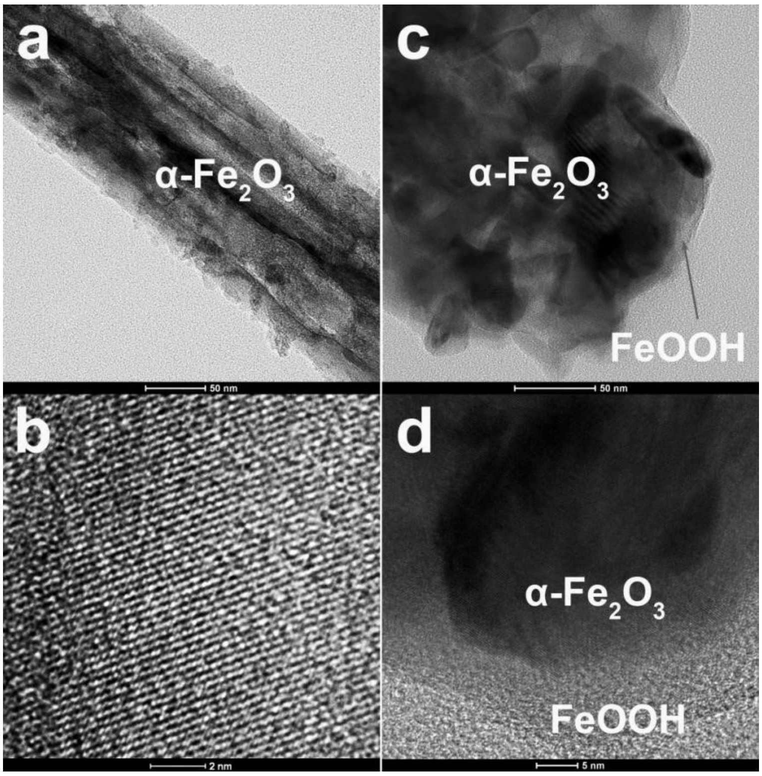

Fig. S4 The TEM and HRTEM images of FTO/Sn@α-Fe_2O_3 (a and b) and FTO/Sn@α-Fe_2O_3/FeOOH (c and d) photoanodes.

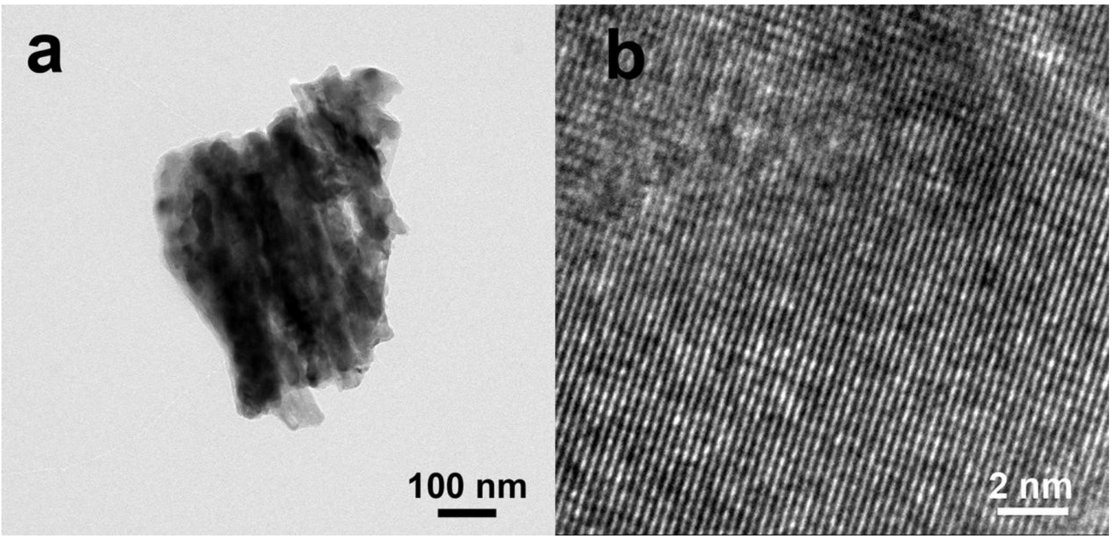

Fig. S5 The TEM and HRTEM images of FTO/Sn@α-Fe_2O_3/FeOOH/TU photoanode.

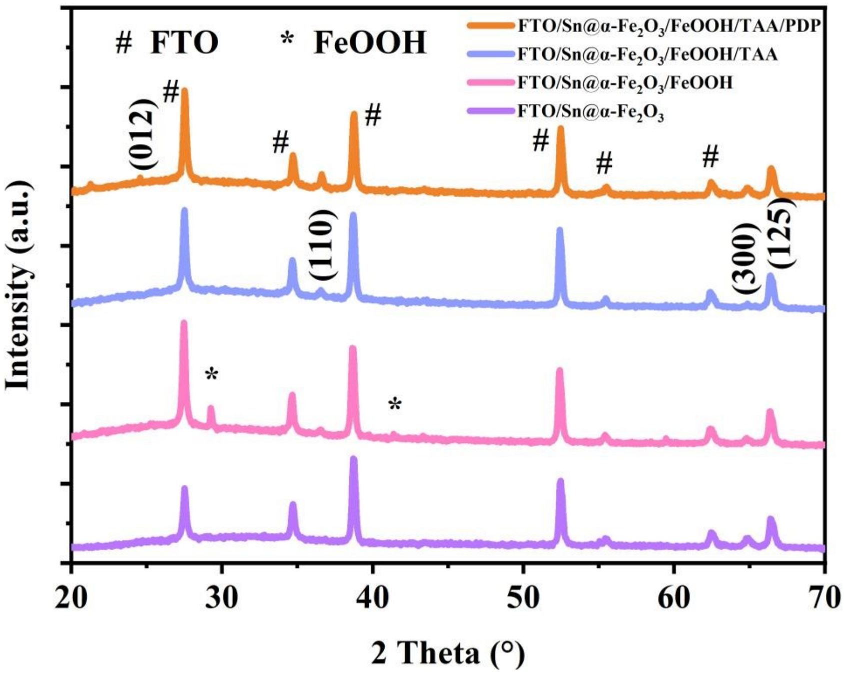

Fig. S6 The XRD patterns of FTO/Sn@α-Fe_2O_3, FTO/Sn@α-Fe_2O_3/FeOOH, FTO/Sn@α-Fe_2O_3/FeOOH/TAA, and FTO/Sn@α-Fe_2O_3/FeOOH/TAA/PDP photoanodes.

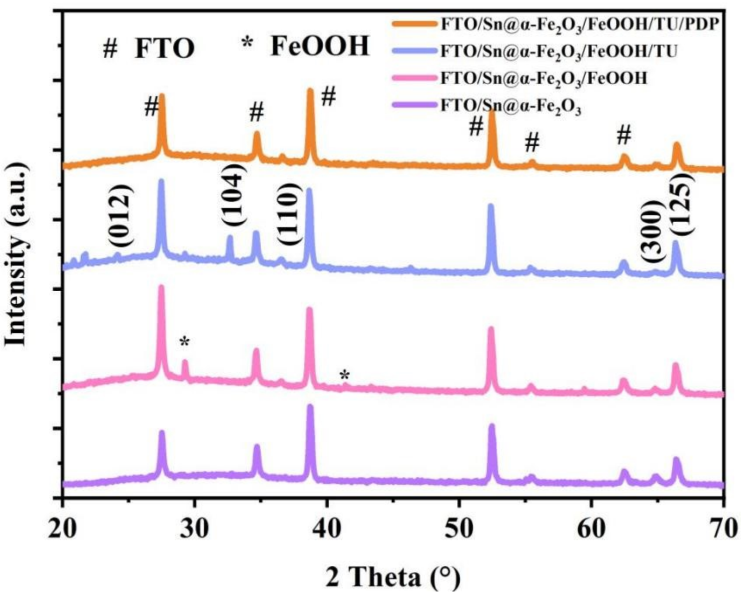

Fig. S7 The XRD patterns of FTO/Sn@α-Fe_2O_3, FTO/Sn@α-Fe_2O_3/FeOOH, FTO/Sn@α-Fe_2O_3/FeOOH/TU, and FTO/Sn@α-Fe_2O_3/FeOOH/TU/PDP photoanodes.

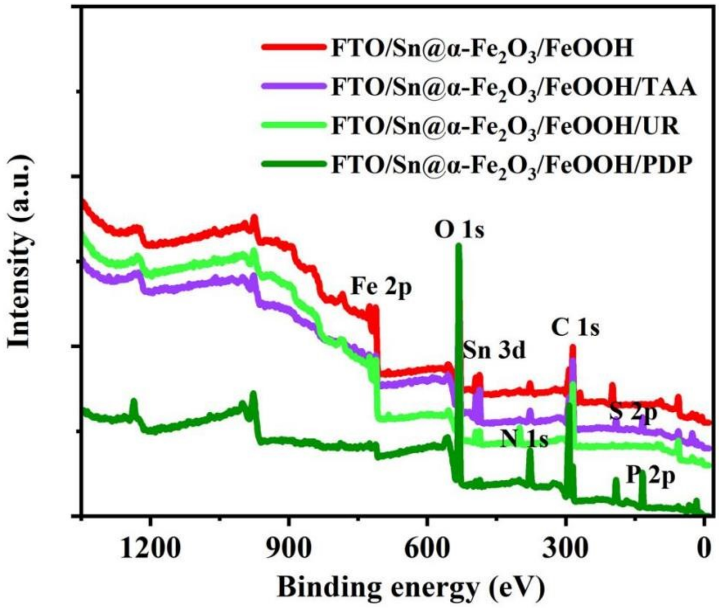

Fig. S8 The XPS spectra of FTO/Sn@α-Fe_2O_3/FeOOH, FTO/Sn@α-Fe_2O_3/FeOOH/TAA, FTO/Sn@α-Fe_2O_3/FeOOH/UR, and FTO/Sn@α-Fe_2O_3/FeOOH/PDP photoanodes.

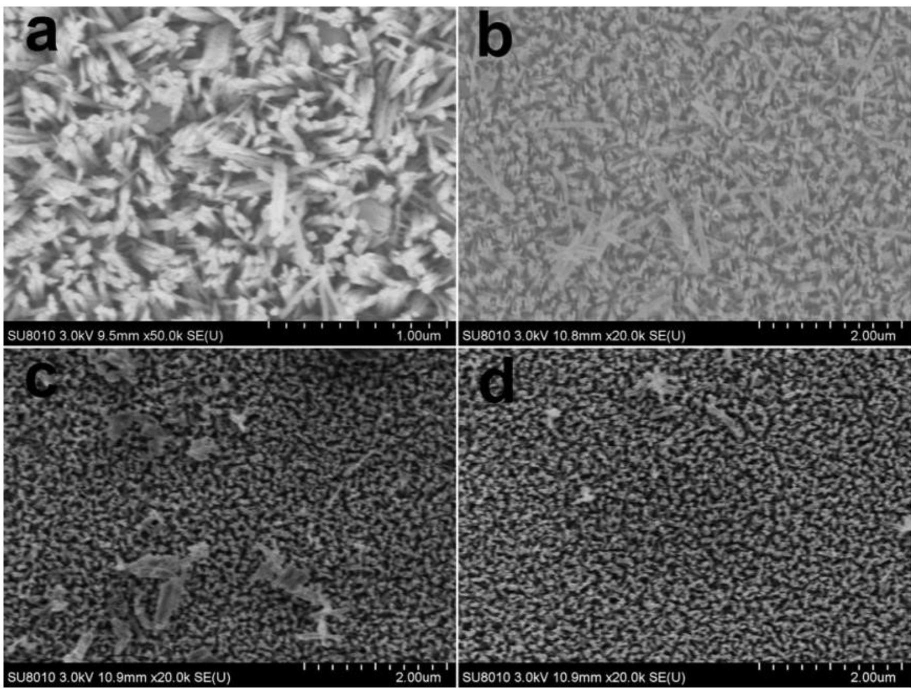

Fig. S9 The top-view SEM images of (a) FTO/Sn@α-Fe_2O_3, (b) FTO/Sn@α-Fe_2O_3/TAA-30s, (c) FTO/Sn@α-Fe_2O_3/TAA-60s, and (d) FTO/Sn@α-Fe_2O_3/TAA-5min photoanodes, respectively.

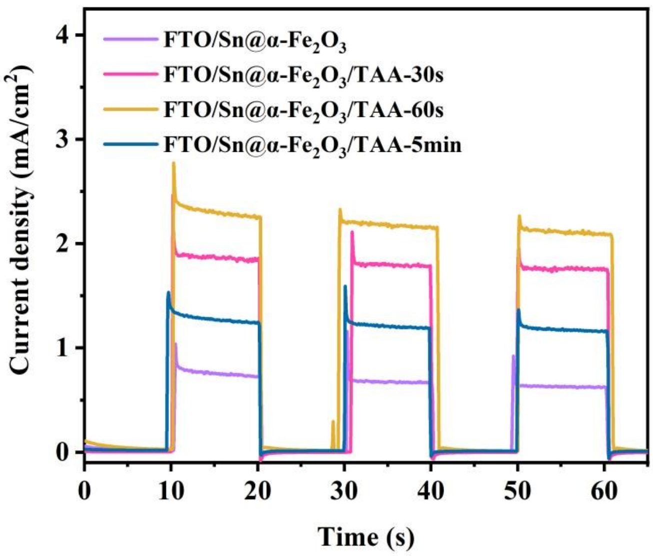

Fig. S10 The transient photocurrent density curves of FTO/Sn@α-Fe_2O_3, FTO/Sn@α-Fe_2O_3/TAA-30s, FTO/Sn@α-Fe_2O_3/TAA-60s, and FTO/Sn@α-Fe_2O_3/TAA-5min photoanodes, respectively.

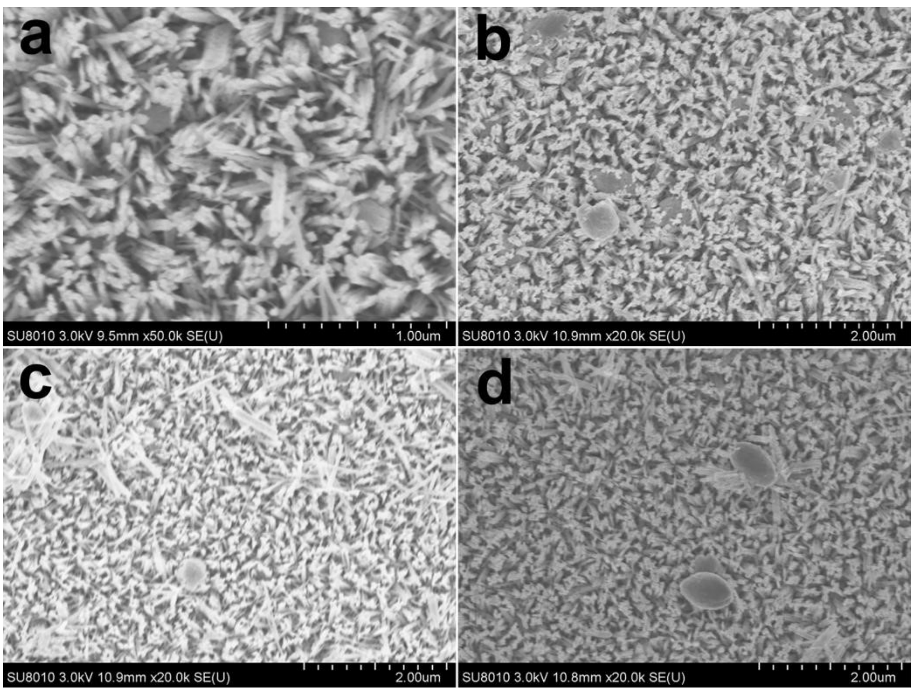

Fig. S11 The top-view SEM images of (a) FTO/Sn@α-Fe_2O_3, (b) FTO/Sn@α-Fe_2O_3/UR-30s, (c) FTO/Sn@α-Fe_2O_3/UR-60s, and (d) FTO/Sn@α-Fe_2O_3/UR-5min photoanodes, respectively.

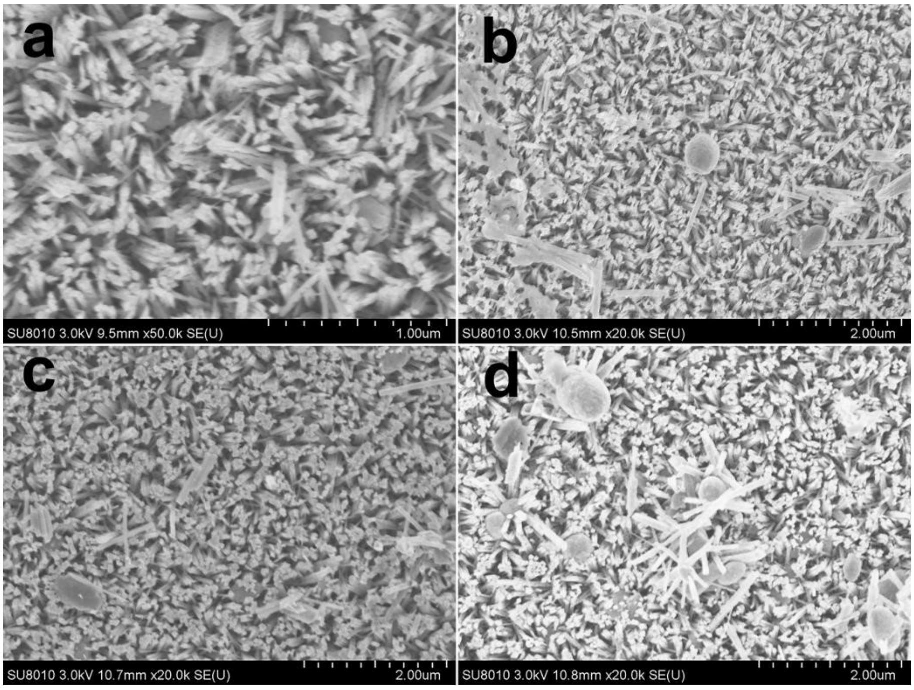

Fig. S12 The top-view SEM images of (a) FTO/Sn@α-Fe_2O_3, (b) FTO/Sn@α-Fe_2O_3/PDP-30s, (c) FTO/Sn@α-Fe_2O_3/PDP-60s, and (d) FTO/Sn@α-Fe_2O_3/PDP-5min photoanodes, respectively.

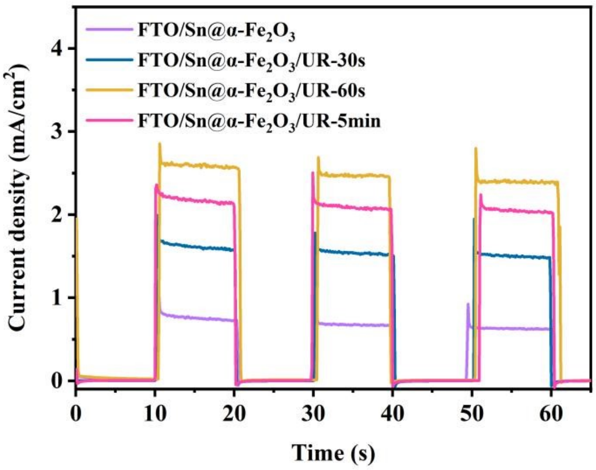

Fig. S13 The transient photocurrent density curves of FTO/Sn@α-Fe_2O_3, FTO/Sn@α-Fe_2O_3/UR-30s, FTO/Sn@α-Fe_2O_3/UR-60s, and FTO/Sn@α-Fe_2O_3/UR-5min photoanodes, respectively.

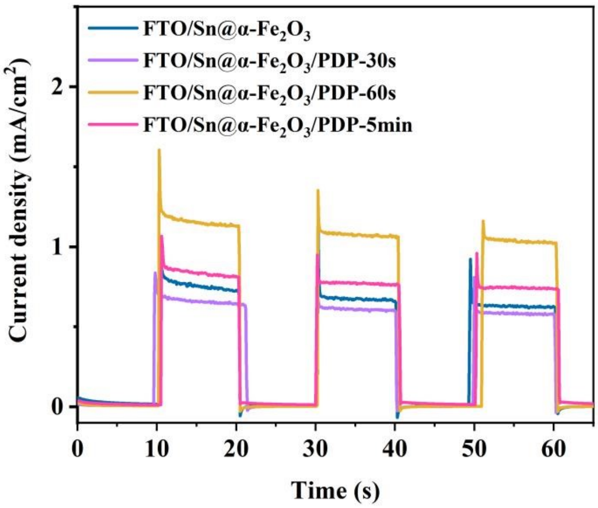

Fig. S14 The transient photocurrent density curves of (a) FTO/Sn@α-Fe_2O_3, (b) FTO/Sn@α-Fe_2O_3/PDP-30s, (c) FTO/Sn@α-Fe_2O_3/PDP-60s, and (d) FTO/Sn@α-Fe_2O_3/PDP-5min photoanodes, respectively.

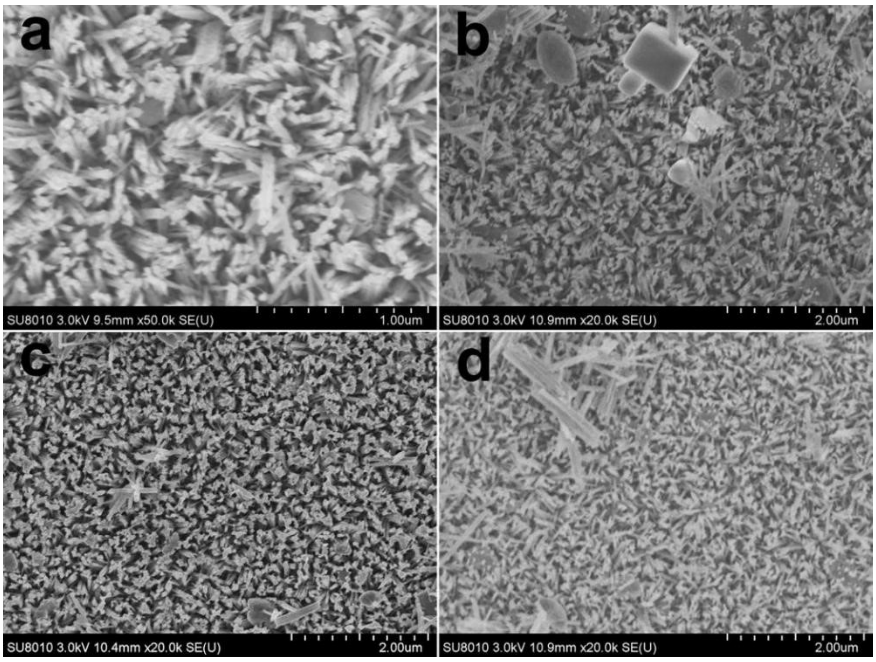

Fig. S15 The top-view SEM images of (a) FTO/Sn@α-Fe_2O_3, (b) FTO/Sn@α-Fe_2O_3/TU-30s, (c) FTO/Sn@α-Fe_2O_3/TU-60s, and (d) FTO/Sn@α-Fe_2O_3/TU-5min photoanodes, respectively.

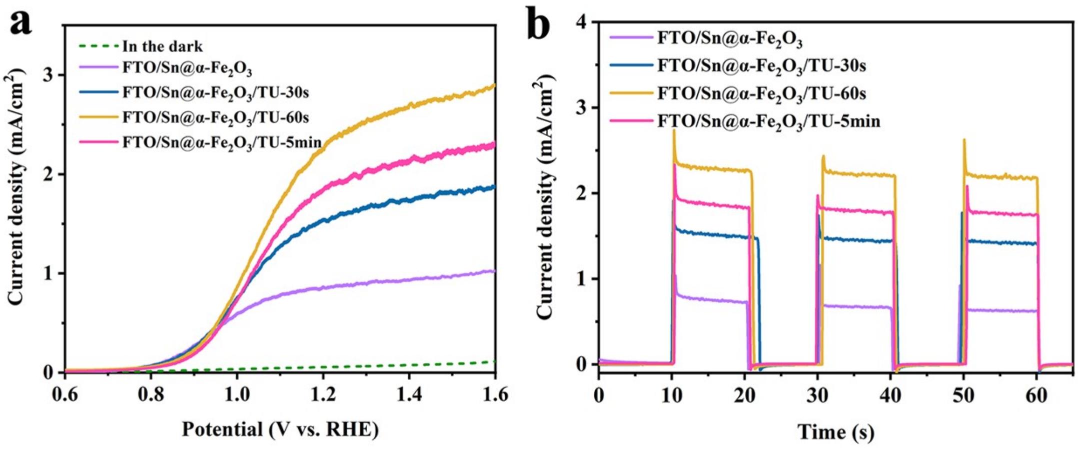

Fig. S16 The (a) *J-V* curves and (b) transient photocurrent density curves of FTO/Sn@α-Fe_2O_3, FTO/Sn@α-Fe_2O_3/TU-30s, FTO/Sn@α-Fe_2O_3/TU-60s, and FTO/Sn@α-Fe_2O_3/TU-5min photoanodes, respectively.

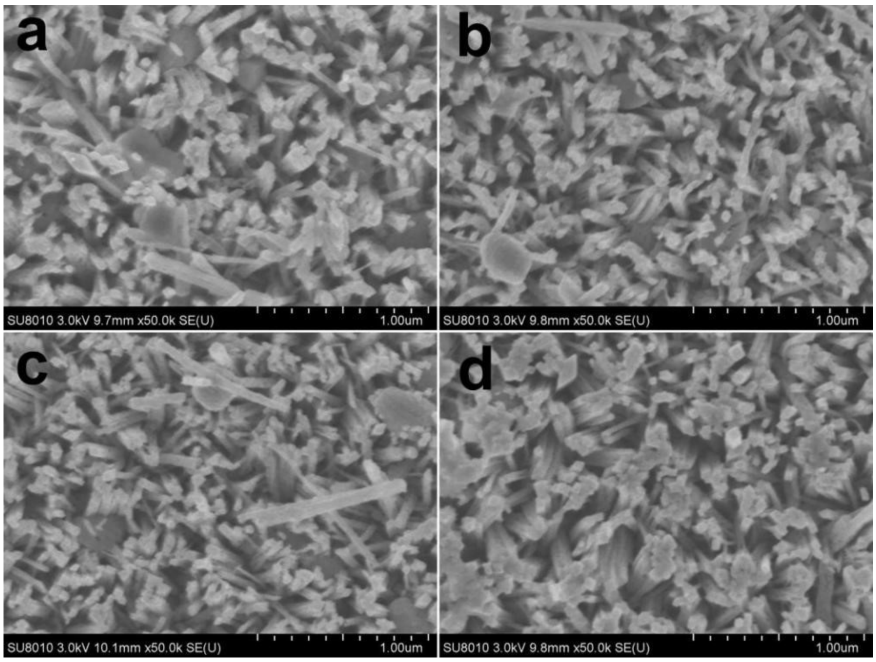

Fig. S17 The top-view SEM images of (a) FTO/Sn@α-Fe_2O_3/FeOOH-1, (b) FTO/Sn@α-Fe_2O_3/FeOOH-3, (c) FTO/Sn@α-Fe_2O_3/FeOOH-5, and (d) FTO/Sn@α-Fe_2O_3/FeOOH-7 photoanodes, respectively.

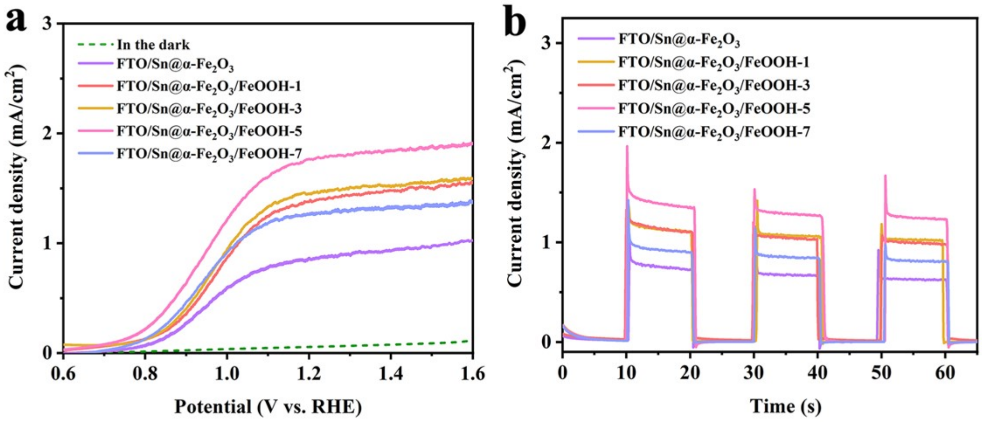

Fig. S18 The (a) *J-V* curves and (b) transient photocurrent density curves of FTO/Sn@α-Fe_2O_3, FTO/Sn@α-Fe_2O_3/FeOOH-1, FTO/Sn@α-Fe_2O_3/FeOOH-3, FTO/Sn@α-Fe_2O_3/FeOOH-5, and FTO/Sn@α-Fe_2O_3/FeOOH-7 photoanodes.

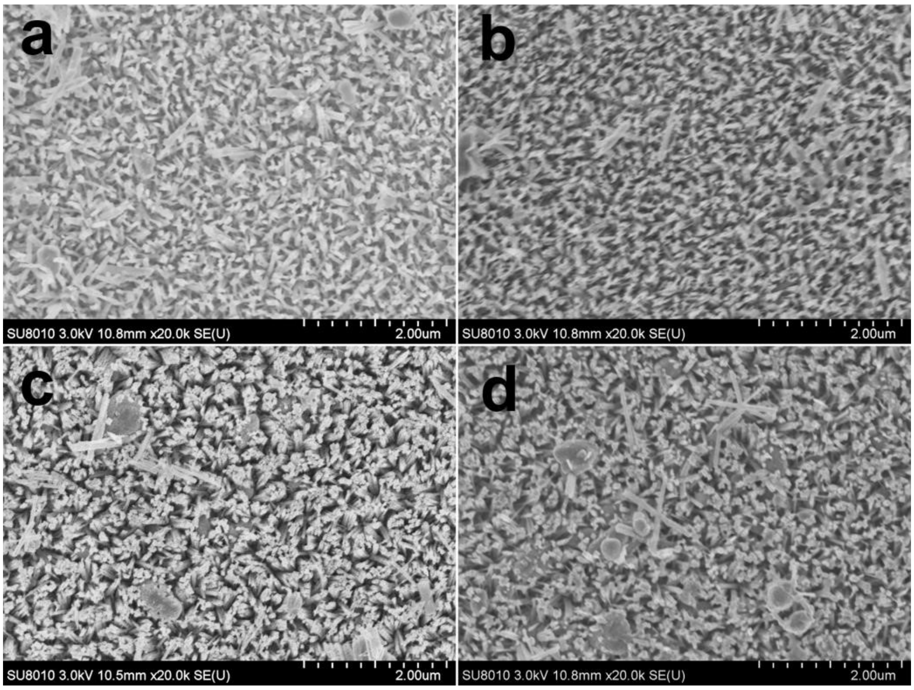

Fig. S19 The top-view SEM images of (a) FTO/Sn@α-Fe_2O_3/FeOOH/TAA, (b) FTO/Sn@α-Fe_2O_3/FeOOH/TAA/PDP, (c) FTO/Sn@α-Fe_2O_3/FeOOH/TU, and (d) FTO/Sn@α-Fe_2O_3/FeOOH/TU/PDP photoanodes, respectively.

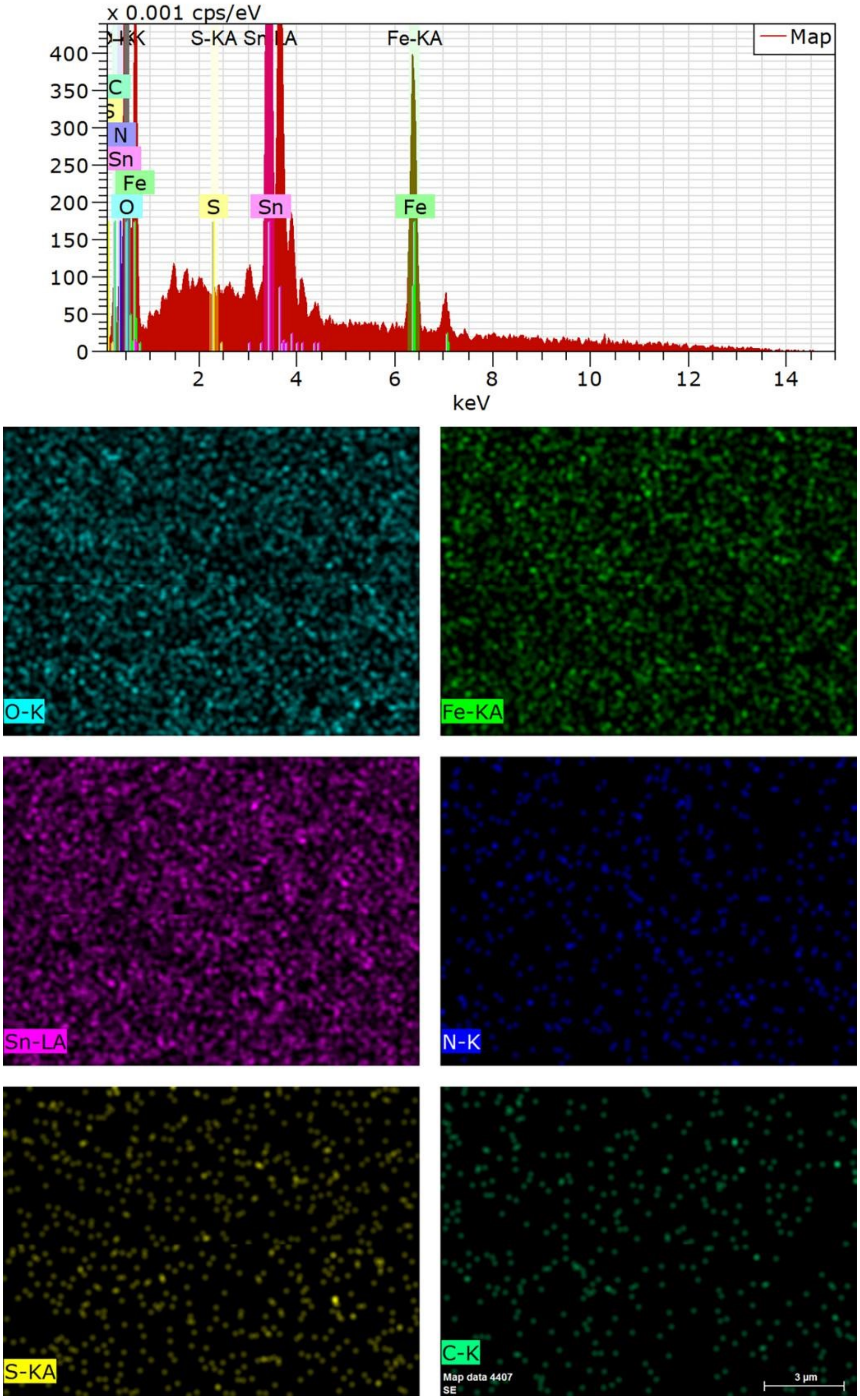

Fig. S20 The EDS composition of FTO/Sn@α-Fe_2O_3/FeOOH/TAA photoanode.

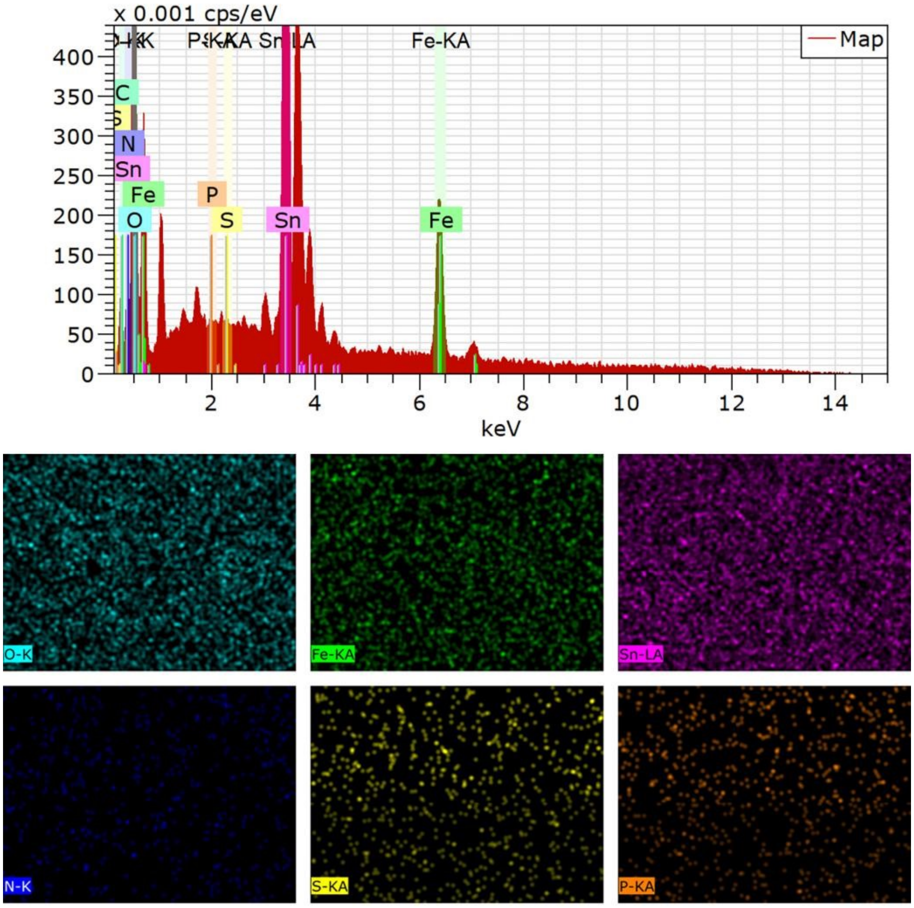

Fig. S21 The EDS composition of FTO/Sn@α-Fe_2O_3/FeOOH/TAA/PDP photoanode.

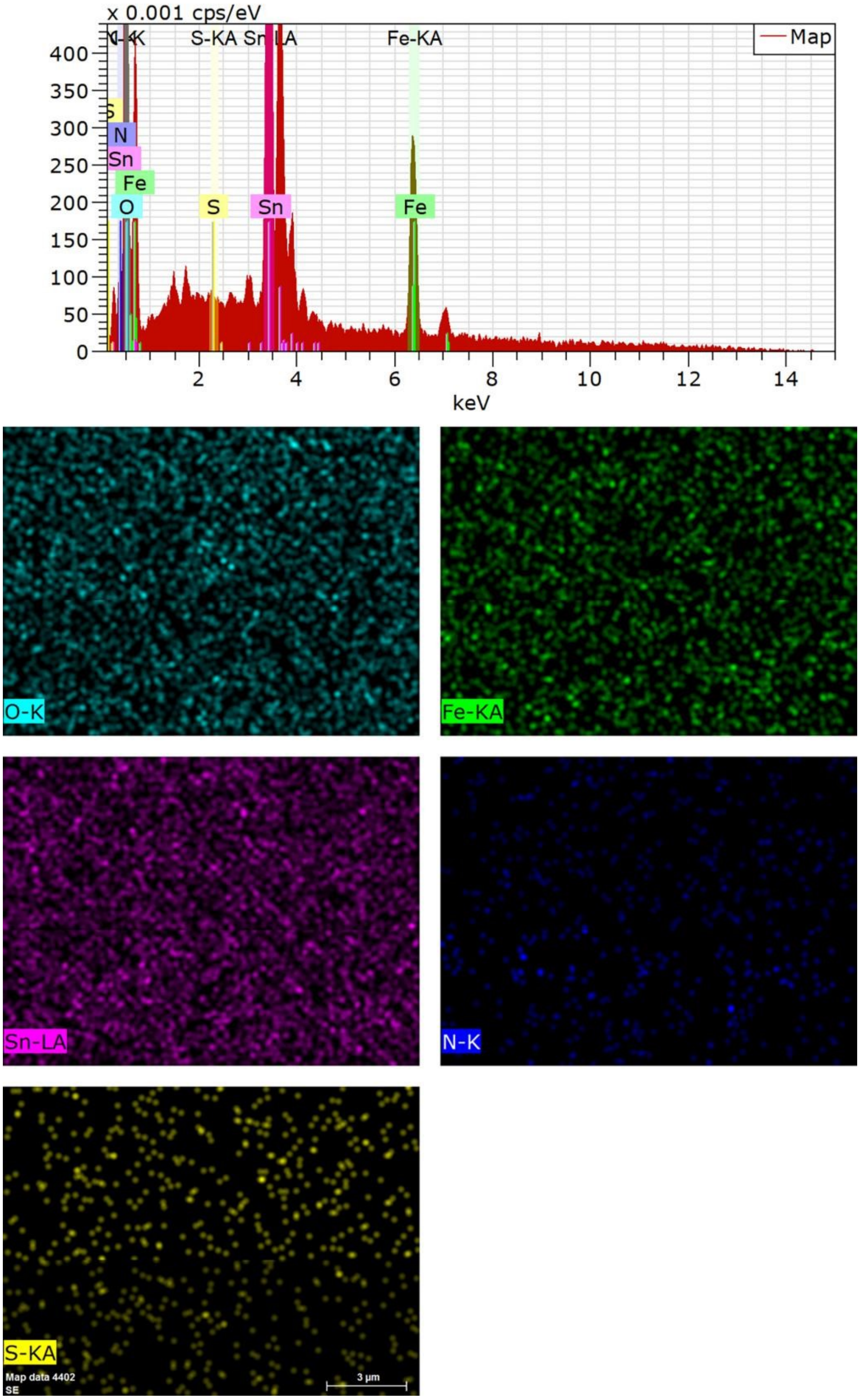

Fig. S22 The EDS composition of FTO/Sn@α-Fe_2O_3/FeOOH/TU photoanode.

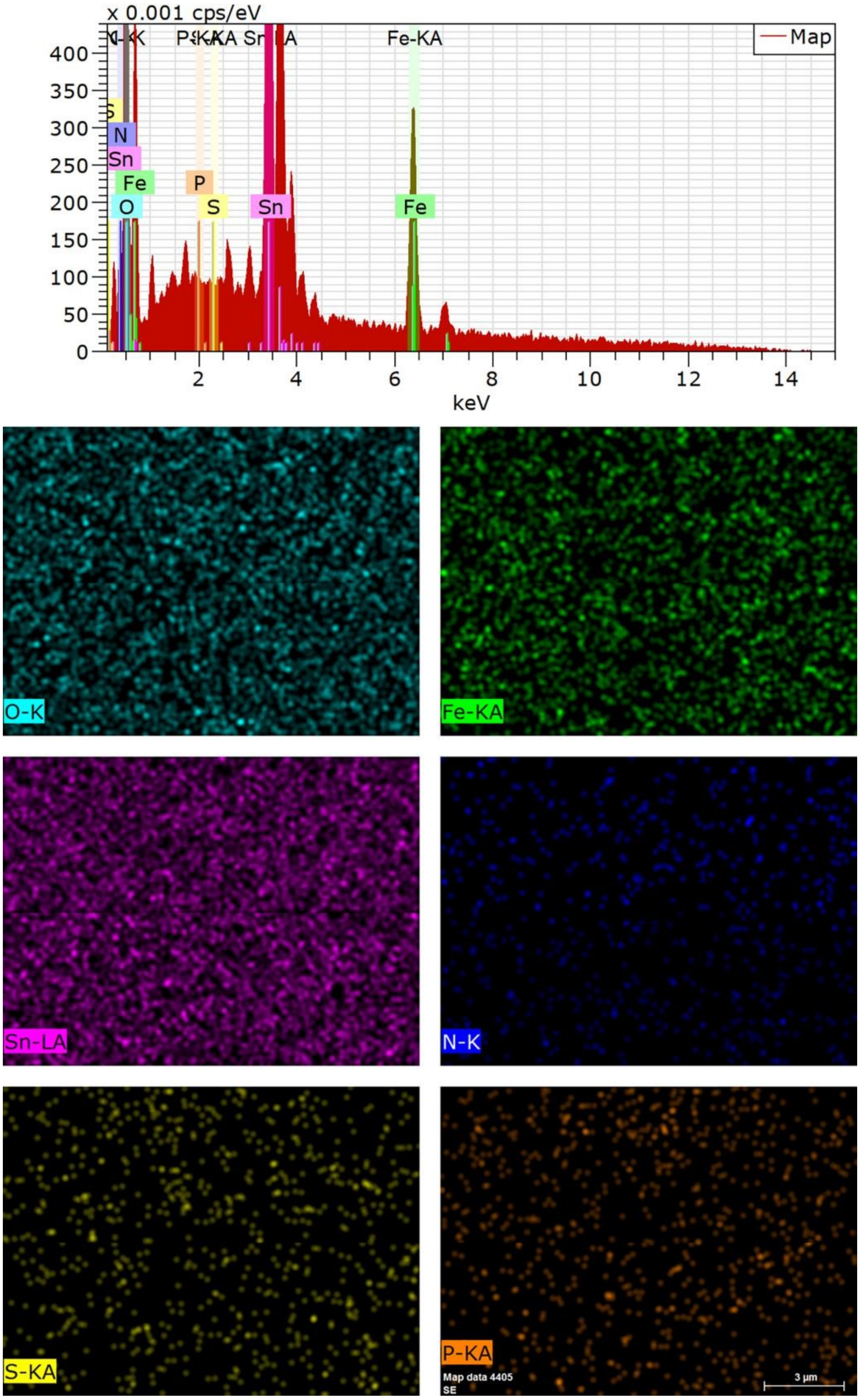

Fig. S23 The EDS composition of FTO/Sn@α-Fe_2O_3/FeOOH/TU/PDP photoanode.

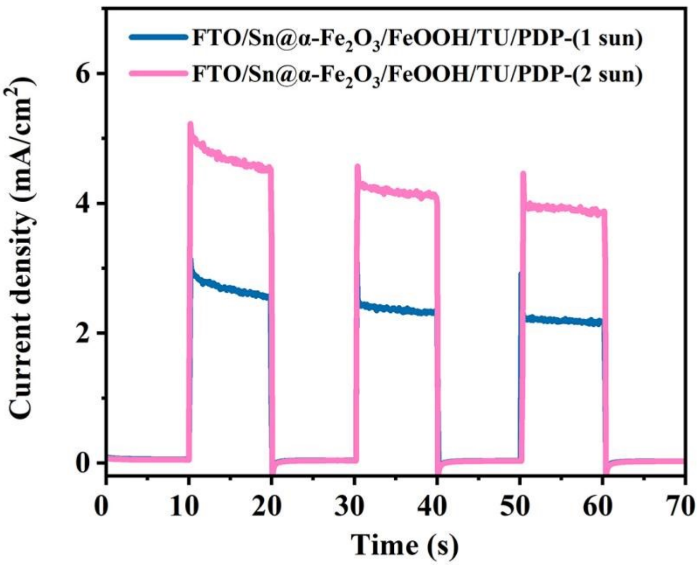

Fig. S24 The transient photocurrent density curves of FTO/Sn@α-Fe_2O_3/FeOOH/TU/PDP photoanode with different light intensity (1 sun and 2 sun).

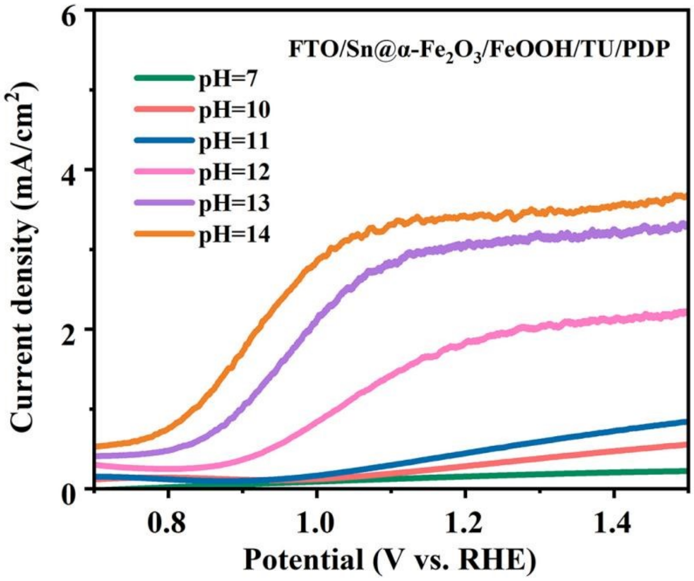

Fig. S25 The *J-V* curves of FTO/Sn@α-Fe_2O_3/FeOOH/TU/PDP photoanode with different pH.

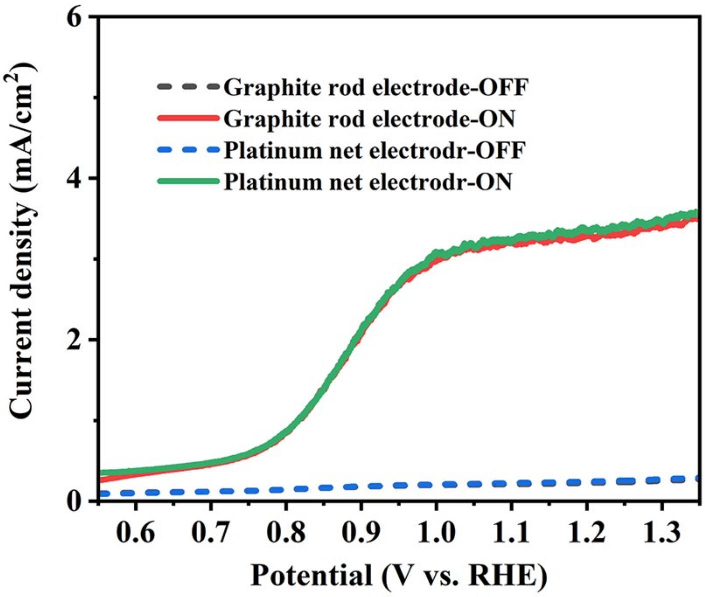

Fig. S26 A comparison of *J-V* curves for FTO/Sn@α-Fe_2O_3/FeOOH/TU/PDP photoanode using platinum mesh and graphite rod as the counter electrode, respectively.

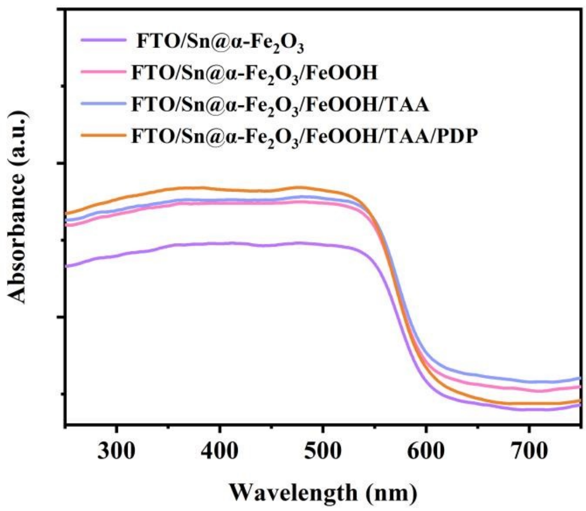

Fig. S27 The UV-vis absorbance spectra of FTO/Sn@α-Fe_2O_3, FTO/Sn@α-Fe_2O_3/FeOOH, FTO/Sn@α-Fe_2O_3/FeOOH/TAA, and FTO/Sn@α-Fe_2O_3/FeOOH/TAA/PDP photoanodes.

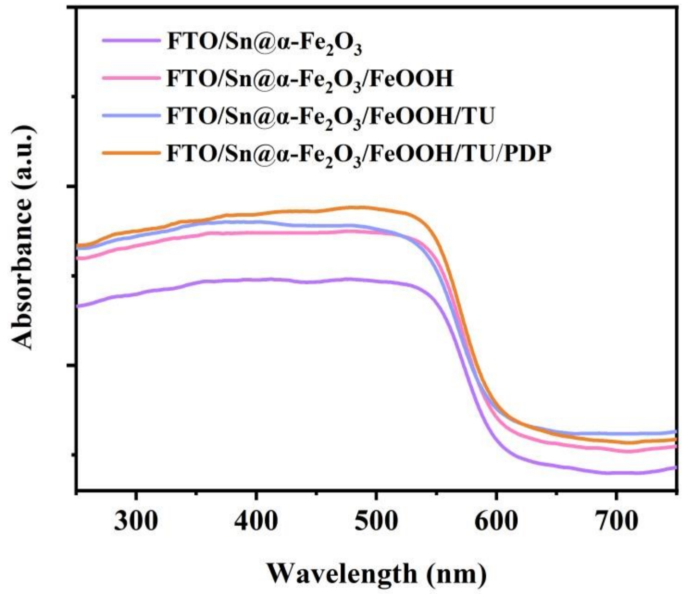

Fig. S28 The UV-vis absorbance spectra of FTO/Sn@α-Fe_2O_3, FTO/Sn@α-Fe_2O_3/FeOOH, FTO/Sn@α-Fe_2O_3/FeOOH/TU, and FTO/Sn@α-Fe_2O_3/FeOOH/TU/PDP photoanodes.

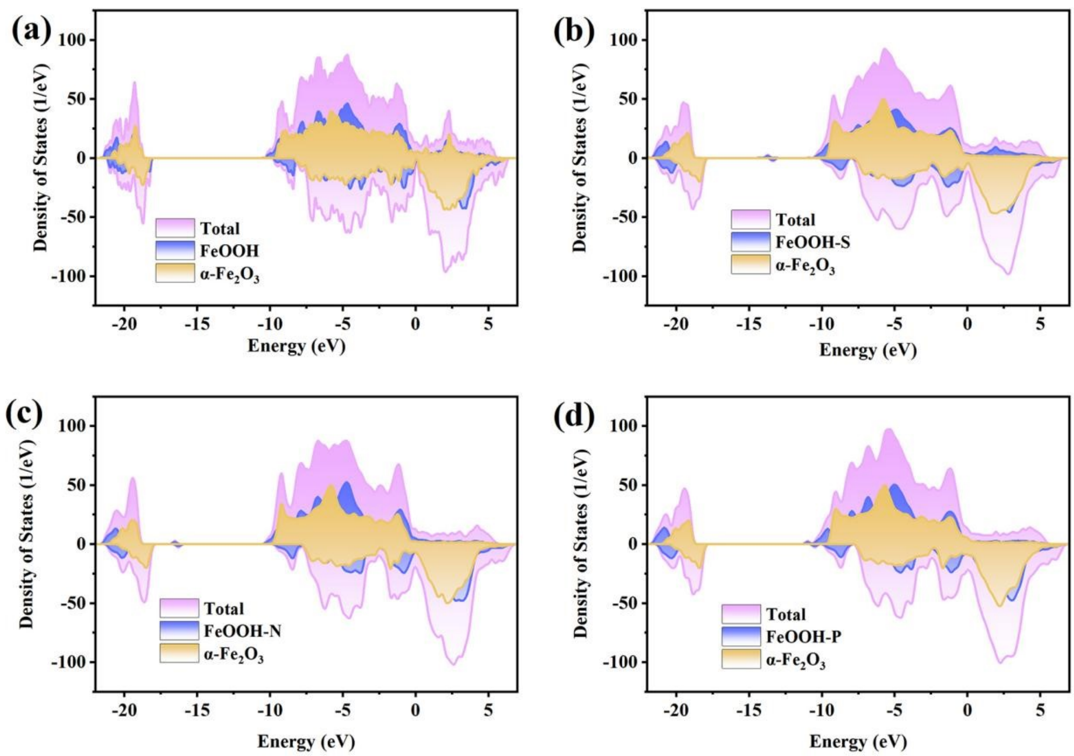

Fig. S29 The density of states in (a) α-Fe_2O_3/FeOOH photoanode with (b) sulfide, (c) nitride, (d) phosphide, respectively.

Tab. S1 A comparison of the PEC-WS performances between hematite photoanodes in the related literature and our present hematite photoanode with in situ sulfide/nitride/phosphide treatments.

Photoanode	**Film texture**	**Optimized sample (*J-V* curves)**	***J*$_{ph@1.23V}$ *U*$_{on}$**	**Testing conditions (Under AM1.5G irradiation)**	**Key Methods**	**Ref.**
NiCoAl-LDH/α-Fe_2O_3	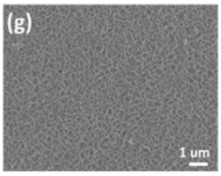	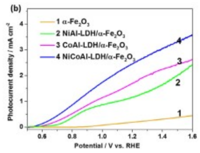	2.56 mA/cm^2 0.55 V_{RHE}	0.5 M potassium phosphate (K-Pi) buffer (pH = 7)	hydrothermal method	[1]
FTO/Sn@α-Fe_2O_3-Mn/CoO_x	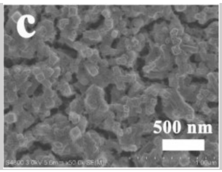	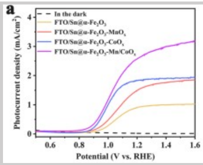	2.67 mA/cm^2 0.8 V_{RHE}	1 M NaOH (pH 13.6) with 20 mV/s	hydrothermal method and annealing	[2]
Co-Pi/Co_3O_4/Ti:Fe_2O_3	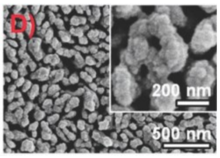	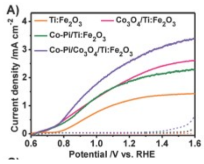	2.7 mA/cm^2 0.64 V_{RHE}	1 M NaOH (pH 13.6)	hydrothermal and electrodeposition	[3]
Pt:Fe_2O_3/Co-Pi	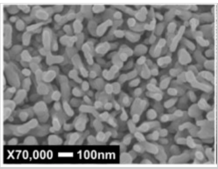	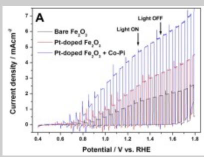	4.32 mA/cm^2 0.58 V_{RHE}	1 M NaOH (pH 13.6)	solution-based method	[4]
α-Fe_2O_3/Ni_3FeOOH/Ag@SiO_2/FeOOH-5	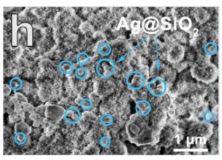	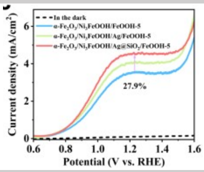	4.54 mA/cm^2 0.7 V_{RHE}	1 M NaOH (pH 13.6) with 20 mV/s	hydrothermal method and spin-coated	[5]
SiMWs/Sn@α-Fe_2O_3 with RTP	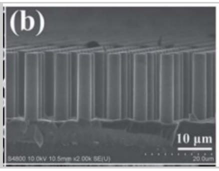	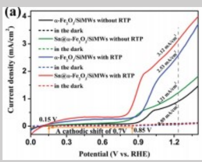	3.12 mA/cm^2 0.15 V_{RHE}	1 M NaOH (pH 13.6) with 20 mV/s	thermal decomposition and RTP	[6]
α-Fe_2O_3/n-SiNWs	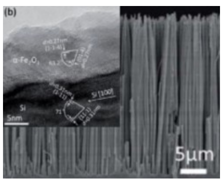	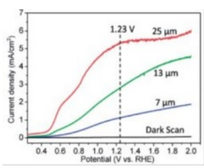	5.28 mA/cm^2 0.50 V_{RHE}	1 M NaOH (50 mV/s) with magnetic stirring	deposition annealing	[7]
FTO/Sn@α-Fe_2O_3	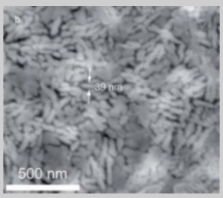	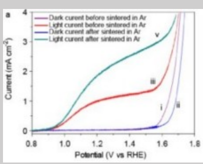	2.30 mA/cm^2 0.80 V_{RHE}	1 M NaOH	thermal posttreatment under Ar gas at 550 °C	[8]

					for 6 hours	
SAs Pt:Fe_2O_3	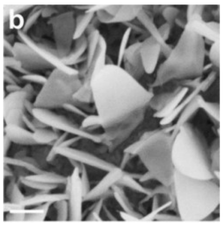	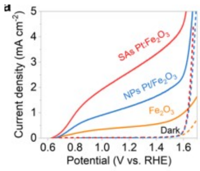	2.71 mA/cm^2 0.627 V_{RHE}	1 M Potassium hydroxide (KOH, pH = 14) with 10 mV/s	thermally annealed and plasma etching	[9]
DASs Ru-P:Fe_2O_3	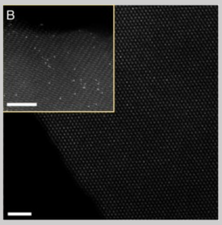	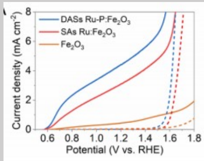	3.32 mA/cm^2 0.63 V_{RHE}	1 M Potassium hydroxide (KOH, pH = 14) with 10 mV/s	thermally annealed and CVD	[10]
FTO/Sn@α-Fe_2O_3/FeOOH/ TAA/PDP	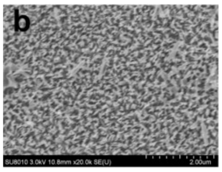	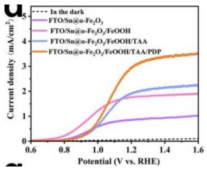	3.09 mA/cm^2 0.8 V_{RHE}	1 M NaOH (pH 13.6) with 20 mV/s	Hydrothermal, electrodeposition and in situ sulfide/phosphide	**This work**
FTO/Sn@α-Fe_2O_3/FeOOH/ TU/PDP	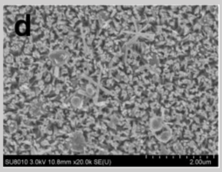	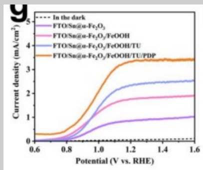	3.38 mA/cm^2 0.7 V_{RHE}	1 M NaOH (pH 13.6) with 20 mV/s	Hydrothermal, electrodeposition and in situ sulfide/nitride/ phosphide	**This work**

References

[1] G. Wang, B. Wang, C. Su, D. Li, L. Zhang, R. Chang and Z. Chang, *J. Catal.*, 2018, **359**, 287–295.

[2] X.-S. Xing, M. Bao, P. Wang, X. Wang, Y. Wang and J. Du, *Appl. Sur. Sci.*, 2022, **572**, 151472.

[3] S.-S. Yi, B.-R. Wulan, J.-M. Yan and Q. Jiang, *Adv. Funct. Mater.*, 2019, **29**, 1801902.

[4] J. Y. Kim, G. Magesh, D. H. Youn, J.-W. Jang, J. Kubota, K. Domen and J. S. Lee, *Sci. Reports*, 2013, **3**, 268.

[5] X.-S. Xing, X. Ren, X. Zeng, A. Li, Y. Wang, Z. Zhou, Y. Guo, S. Wu and J. Du, *Sol. RRL*, 2023, **7**, 2201041.

[6] Z. Zhou, S. Wu, L. Qin, L. Li, L. Li and X. Li, *J. Mater. Chem. A*, 2018, **6**,

15593–15602.

[7] X. Qi, G. She, X. Huang, T. Zhang, H. Wang, L. Mu and W. Shi, *Nanoscale*, 2014, **6**, 3182–3189.

[8] J. J. Wang, Y. Hu, R. Toth, G.Fortunato and A. Braun, *J. Mater. Chem. A*, 2016, **4**, 2821–2825.

[9] R.-T. Gao, J. Zhang, T. Nakajima, J. He, X. Liu, X. Zhang, L. Wang and L. Wu, *Nat. Commun.*, 2023, **14**, 2640.

[10] R.-T. Gao, L. Liu, Y. Li, Y. Yang, J. He, X. Liu, X. Zhang, L. Wang and L. Wu, *Proc. Natl. Acad. Sci. USA*, 2023, **120**, e2300493120.